www.czasopisma.pan.pl PAN POLSKA AKADEMIA NAUK www.journals.pan.pl

Metrol. Meas. Syst., Vol. XVII (2010), No. 4, pp. 621–636

PAN POLSKA AKADEMIA NAUK

METROLOGY AND MEASUREMENT SYSTEMS

Index 330930, ISSN 0860-8229

www.metrology.pg.gda.pl

M&MS

APPROXIMATION OF THERMAL BACKGROUND APPLIED TO DEFECT DETECTION USING THE METHODS OF ACTIVE THERMOGRAPHY

Sebastian Dudzik

Czestochowa University of Technology, Faculty of Electrical Engineering, Al. Armii Krajowej 17, 42-200 Częstochowa, Poland
(✉ sebdud@el.pcz.czest.pl, +48 34 325 0856*)*

Abstract

In the paper a method for correction of heating non-homogeneity applied in defect detection with the use of active thermography is presented. In the method an approximation of thermal background with second- and third -order surfaces was used, what made it possible to remove partially the background. In the paper the simulation results obtained with the abovementioned method are presented. An analysis of the influence of correction of heating non-homogeneity on the effectiveness of defect detection is also carried out. The simulations are carried out for thermograms obtained on the basis of experiments on a test sample with simulated defects, made of a material of low thermal diffusivity.

Keywords: active thermography, non-destructive testing, heating non-homogeneity correction.

1. Active thermography in infrared range

1.1. Introduction

Contemporary thermography in infrared range makes it possible both to depict and to measure temperatures on the surfaces of examined bodies [1–3]. Making use of complicated measurement models allows one to determine precisely the accuracy of temperature determination with thermovision methods [1], [4–6]. Taking the abovementioned feature into account, it can be stated that thermovision in the infrared range is a promising research tool for numerous branches of science and technology, *e.g.* medicine, civil engineering or power engineering [3].

Within the framework of thermography in infrared range, passive and active procedures can be distinguished. In the passive procedure the infrared radiation emitted by a body not subjected to thermal stimulation (heating). The active procedure relies in heating of the examined body and recording of the thermal field on its surface. A specific case of active thermography is active dynamic thermography, when recording is applied to transient temperature field. Active thermography has found a wide application scope in nondestructive testing of materials, in particular in defect detection [7–11]. For recording of the temperature field on the surface of the examined body an infrared camera may be used [1]. However, it constitutes just the first component of the measurement path which makes it possible to record individual thermograms or their sequences. In order to record sequences, the camera has to be supplied with a frame grabber and appropriate digital interfaces. Additionally, in nondestructive testing methods making use of active thermography, a specialized software is used. Usually the pieces of software are installed on a PC-class computer.

Article history: received on Jul. 20, 2010; accepted on Nov. 12, 2010; available online on Nov. 26, 2010; DOI: 10.2478/v10178-010-0051-3.

1.2. Testing procedures in active thermography

The foundation of contemporary active thermography is the equation of thermal wave [12]. In the case of semi-finite body subjected to periodical thermal excitation, this equation makes it possible to determine the value of temperature at the depth z (m) for the instant τ (s) [12]:

$$T(z,\tau) = T_0 e^{-z/\mu} \cos\left(\Omega\tau - \frac{2\pi z}{\lambda}\right) \text{ (K)}, \tag{1}$$

where: T_0 (K) – temperature on sample surface (for z = 0), Ω – angular frequency of periodical thermal excitation (rad s^{-1}), $\lambda = 2\pi\mu$ (m) – length of thermal wave, $\mu = \sqrt{2\alpha/\Omega}$ (m) – length of the diffusion path, α (m^2 s^{-1}) – thermal diffusivity of the sample material. The simplest procedure to detect defects in the surface layer of material is pulsed thermography [7]. It requires the knowledge of time variation of excess temperature on the surface of the examined sample for thermal excitation given as a Dirac impulse:

$$\Delta T(\tau) = \frac{Q}{e\sqrt{\pi\tau}} \text{ (K)}. \tag{2}$$

In Eq. (2) the following notation is used: ΔT – rise of sample temperature, $e = \sqrt{k\rho C_p}$ (W m^{-2} K^{-1}) – thermal effusivity of sample material, k (W m^{-1} K^{-1}) – thermal conductivity, ρ (kg m^{-3}) – material density, C_p (J kg^{-1} K^{-1}) – specific heat of material, Q (J m^{-2}) – density of impulse energy. The existence of a defect in the surface layer of the material is indicated by the difference between the recorded temperature transient and the transient obtained on the basis of relationship (2) for the measured value of material effusivity and fixed value of energy of the supply source.

The analytical solution of the afore-described case may be found e.g. in References [7], [13]. A semi-finite plate spans in the space up to infinity along the x and y axes, but it possesses a finite thickness along the z axis ($0 \le z \le l$). Both plate surfaces are thermally insulated, but the side at z = 0 has been subjected to a thermal Dirac impulse, uniform for the whole surface. In order to obtain an analytical solution it is assumed that for τ = 0 the plate temperature is equal to zero (there is no temperature difference between the plate and ambient surrounding), but in the region close to the plate surface ($0 \le z \le z_e$, $z_e << l$) the plate temperature is equal to T_0. Taking the geometry into account, the Fourier equation may be reduced to a dimensionless equivalent. Then $T(z,\tau)$ corresponds to temperature distribution at depth z for the instant τ and is given by the following relationship [13]:

$$T(z,t) = T_f\left[1 + \frac{21}{\pi z_e}\sum_{n=1}^{\infty}\frac{1}{n}\sin\frac{n\pi z_e}{l}\cos\frac{n\pi z}{l}\exp\left(\frac{-t\alpha^2\pi^2n^2}{l^2}\right)\right] \text{ (K)}, \tag{3}$$

where: $T_f = T_0 z_e / l$ – final temperature for the heat exchange process (for $\tau \to \infty$).

From Eq. (3) it follows that even for such a simplified geometry, the analytical solution is rather complex. When considering either anisotropic properties or subsurface defects, the analytical approach quickly becomes useless, particularly in those cases when a dimensionless approximation cannot be obtained. From the point of view of experimental practice, the obtainment of either a periodical or an impulse excitation may be troublesome. Therefore in experimental tests carried out within the scope of the present work the stepped heating method (also known as time-resolved infrared radiometry) was used [7, 10, 11]. In the method, the increase of surface temperature is monitored during the whole duration time of

Metrol. Meas. Syst., Vol. XVII (2010), No. 4, pp. 00–00

excitation (the sample is heated continuously at low excitation power). Let us assume that the sample geometry consists of two material layers of different thermal properties. The schematic depiction is given in Fig. 1 [7].

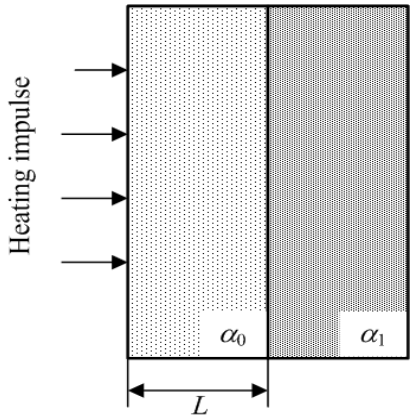

Fig. 1. Two-layer model of the sample [7].

In such situation the second sample layer may represent a subsurface material defect. For such a geometry, the temperature evolution on the heated surface caused by the above-described excitation is given by the relationship:

$$T(\tau) = C_c\sqrt{\tau}\left\{1+\sum_{n=1}^{\infty}2(-\Gamma)^n\left[\exp\left(-\frac{n^2L^2}{\alpha_0\tau}\right)-\frac{nL\sqrt{\pi}}{\sqrt{\alpha_0\tau}}\operatorname{erfc}\left(\frac{nL}{\sqrt{\alpha_0\tau}}\right)\right]\right\}\ \text{(K)}. \tag{4}$$

The constant component C_c is related to energy absorption. For example, for laser heating C_c is given as:

$$C_c = \frac{\varepsilon(1-R)I}{4\pi^{3/2}e_0}, \tag{5}$$

where: ε – emissivity of sample surface, for the wavelength recorded by the camera, R – reflection coefficient for a given laser wavelength, I – laser light intensity. Finally, in the formula (4) a factor Γ occurs, defined as [7]:

$$\Gamma = \frac{e_1 - e_0}{e_1 + e_0}, \tag{6}$$

where e_0 and e_1 determine the effusivities of the first and the second layer, respectively. The Γ coefficient is referred to as thermal mismatch factor between two adjacent layers of material. In the case when the second layer possesses a substantially lower thermal effusivity than the surface layer, the value of the thermal mismatch factor approaches –1. Such situation occurs *e.g.* when an air layer (inclusion) occurs between two metal layers. The above-given equation is just a one-dimensional approximation, which is correct in the case of a layer with a substantial cross-dimension (semi-infinite case) as well as for the initial stage of the process, when the thermal diffusion occurs only in the upper layer of the sample for which the summation factor in the Eq. (4) possesses a low value. The advantage of the method of stepped thermal impulse is the possibility to examine materials of low thermal diffusivity with the use of lower excitation power.

1.3. Approximation of thermal background

Unfortunately, thermograms of examined surfaces recorded with a contemporary infrared camera include noise. Additionally, due to the features of the used sources of thermal excitation, non-uniform heating of the examined surfaces occurs. In practice, for correction of heating non-homogeneity the spatial and temporal reference thermogram techniques are most commonly used [7–9]. The techniques for image processing also improve defect visibility, thus improving its contrast.

The spatial reference thermogram technique is used usually in order to filter repetitive heating non-homogeneity, resulting from the features of the source of thermal excitation. It relies in a comparison of temperature distribution on the surface of a reference sample with temperature distribution on the surface of the examined sample. Both samples are made of the same material. The reference sample does not include defects. The examined sample is suspected to have defects in the sub-surface layer. Both samples are subjected to thermal excitation of the same type. Correction of non-homogeneity is obtained by subtraction of the thermogram of reference sample surface from the thermogram of examined sample surface [7].

Unfortunately in the case of repetitive, time-changing heating non-uniformities, the spatial reference technique does not yield good results. Such conditions occur *e.g.* when surface emissivity changes abruptly or unknown thermal reflections happen. In this case, correction with the use of temporal reference enhancement technique behaves much better. This method relies in subtraction of two thermograms of sequence, representing different time instants. It should be noticed that the image obtained after subtraction of two thermograms represents the variation of the temperature field between two time instants for the heated zone and therefore it is related to thermal properties of the sample, *e.g.* diffusivity.

In the present paper, in order to eliminate heating non-homogeneity and its impact on results of defect detection, another method has been proposed. One of its advantages is the fact that it does not require references necessary for the above-described techniques. In the proposed method of non-homogeneity heating correction, the algorithms used in the technique for image processing in the visible range [14] can be applied. For correction purposes it is assumed that in the analyzed thermal scene, constituting a chosen sequence thermogram consists of two components. The first component is the non-homogenous thermal background. The second component is related with defects occurring in the field of view. The defects may occur at different depths and feature different contrasts. In order to correct non-homogeneity, the approximation of the component representing the thermal background is made. In the present paper, for approximation purposes the following functions of two spatial variables x and y were used:

$$B_2(x,y) = a_0 + a_1x + a_2y + a_3x^2 + a_4y^2 + a_5xy, \tag{7}$$

$$B_3(x,y) = a_0 + a_1x + a_2y + a_3x^2 + a_4xy + a_5y^2 + a_6x^3 + a_7x^2y + a_8xy^2 + a_9y^3. \tag{8}$$

The functions (7), (8) constitute a set of generalized three-dimensional equations of second- and third-order surfaces. The values of coefficients $a_0,\ldots a_5$ in Eq. (7) and the coefficients $a_0\ldots\ a_9$ in Eq. (8) are obtained with the least-square method [15]. The last correction stage is subtraction of the approximated thermal background from the original sequence thermogram, according to the relationship:

$$T_{corr}(x,y) = T(x,y) - B(x,y), \tag{9}$$

Metrol. Meas. Syst., Vol. XVII (2010), No. 4, pp. 00–00

where: $T_{corr}(x, y)$ – temperature value at the pixel with coordinates x, y for the thermogram after correction, $T(x, y)$ – temperature value at the pixel with coordinates x, y for the original thermogram, $B(x, y)$ – value of the approximated thermal background at the pixel with coordinates x, y, obtained with least-square method from Eqs (7), (8). The proposed method has been tested in the subsequent part of the paper.

1.4. Binarization of thermal images

In the present paper, the examination of the above-described method for correction of heating non-homogeneity was carried out. For this purpose the afore-described method was tested on different thermograms, recorded at different stages of the heating and cooling processes. Additionally the approximation parameters *i.e.* the order of the approximation method, were varied. Therefore it was necessary to compare the influence of different options in the method on the capability to detect defects. For this purpose a simple algorithm of automatic defect detection based on binarization of thermal images was applied. Binarization made it possible to compare the correction results obtained with different options of the described method. Additionally, it was possible to compare the detection capability for thermal images with and without correction.

One of important stages of automatic analysis of digital images is its transformation to binary form, which is referred to as binarization [14, 16, 17]. In the course of processing a classification of individual image elements (pixels) is carried out using threshold. As the result of classification, a pixel ordering into one of two groups (objects and background) is obtained. The pixels within the first group (objects) are assigned a unity value, the pixels within the second group (background) are assigned zero value. In the present paper, binarization was carried out in order to classify individual pixels of the thermograms pertaining to the surface of the examined sample into the defect class (unity value) or background class (zero value). The binarization procedure of the thermal image $T(x, y)$ may be written as [14]:

$$J_B(x,y) = \begin{cases} 1 & T(x,y) > v_{th} \\ 0 & T(x,y) \le v_{th} \end{cases}, \tag{10}$$

where: v_{th} – threshold value.

For correct classification of the regions including defects it is extremely important to choose an appropriate threshold value v_{th}. In the present paper the choice of threshold value was carried out using the Otsu method. Subsequently, a short description of the method in reference to intensity images shall be given.

The Otsu method has been formulated on the basis of statistical analysis of images. The threshold v_{th} calculated with this method divides the pixels into two subsets: c_0, which defines the background (here: regions without defects) and c_1, which defines the objects (here: defects). The choice of the optimal threshold value v_{th}* relies in the search for maximum of the criterion function, according to the Eq. [16]:

$$v_{th}^{*} = \arg \max_{0 < v_{th} < L-1} \eta(v_{th}), \tag{11}$$

where "arg" denotes the value of the argument, for which $\eta(v_{th})$ assumes a maximum value, $L-1$ is the total number of intensity levels in the image, whereas the optimized criterion function is defined with the relationship:

$$\eta(v_{th}) = \frac{\sigma_B^2}{\sigma_T^2}, \tag{12}$$

where: σ_B^2 – interclass variation, σ_T^2 – global variation. These variations are given with the following formulas [17]:

$$\sigma_B^2 = P_0 P_1 (\mu_0 - \mu_1)^2, \quad \sigma_T^2 = \sum_{i=0}^{L-1} (i - \mu_T)^2, \tag{13}$$

where: P_0 – probability of occurrence of the pixel class with intensity levels 0, 1, …, v_{th} in the image, P_1 – probability of occurrence of the pixel class with intensity levels v_{th}+1, …, L–1, μ_0, μ_1 – average intensity of the classes c_0 and c_1, respectively, μ_T – average intensity of the whole image. Introducing the threshold value calculated from the relationship (12) into (10), one obtains the binarized image $J_B(x, y)$. In the obtained image, the regions containing pixels with unity value (white pixels) correspond to defects, whereas pixels with zero value (black pixels) belong to the background and do not indicate the occurrence of defects.

2. Experimental research

2.1. Research stand

In the present paper testing of the afore-described method for approximation of thermal background has been carried out. The method has been tested on thermal images recorded during experimental research. The experimental research has been carried out using the stand depicted in Fig. 2. The stand consisted of long-wavelength thermovision camera FLIR ThermaCAM PM595 (1), cooperating with a digital module of communication interface (2) and a PC computer (3) equipped with a frame grabber card and software for real-time acquisition of thermal image sequences [10]. As the source of thermal excitation two modelling lamps (4), 250 W each were used. The examined object was a test sample (5), made of Plexiglas. Its surface was covered with a black, matt lacquer, featuring a high emissivity coefficient ($\varepsilon \approx 0{,}98$). From the bottom side of the sample four non-passing holes were drilled. In this way four defects localized at depths z_1 = 0,5 mm, z_2 = 1,5 mm, z_3 = 2,5 mm and z_4 = 3,5 mm with respect to the upper side of the sample were simulated. The sample dimensions, the location and dimensions of the holes are depicted in Fig. 3 [10].

2.2. Test results

One of the aims of the present paper was to test the above-described method for correction of heating non-homogeneity in reference to thermograms of sequence recorded at different stages of the thermal process. Therefore it was necessary to record both the heating stage and the cooling stage as well. In the experimental tests the above-described method of stepped heating was used. During the tests, the sample surface was heated with a 500 W thermal impulse, duration time 120 s. In order to increase heating homogeneity, two modelling lamps were used, 250 W each. The thermogram sequence was recorded during the heating stage, and subsequently during 120 s of the cooling stage. The sampling frequency was fixed to 5 Hz, and the total number of recorded thermograms was 1200. In Figs 4–6 the results of the described experiment are depicted. The thermal image of the sample surface, recorded at the time instant τ = 32.8 s (beginning of the heating stage) is depicted in Fig. 4, whereas in Figs 5, 6 the thermograms recorded at time instants τ = 120 s (end of heating stage), and τ = 240 s (end of observation of the cooling stage) are shown.

Metrol. Meas. Syst., Vol. XVII (2010), No. 4, pp. 00–00

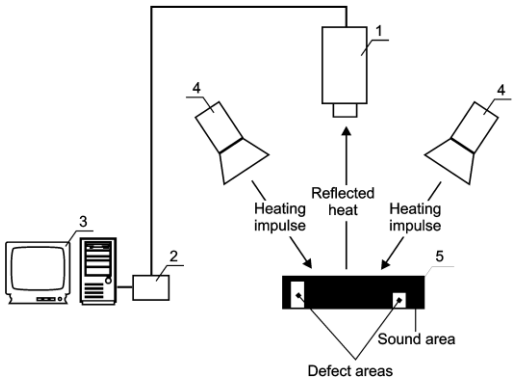

Fig. 2. Depiction of the laboratory stand [10].

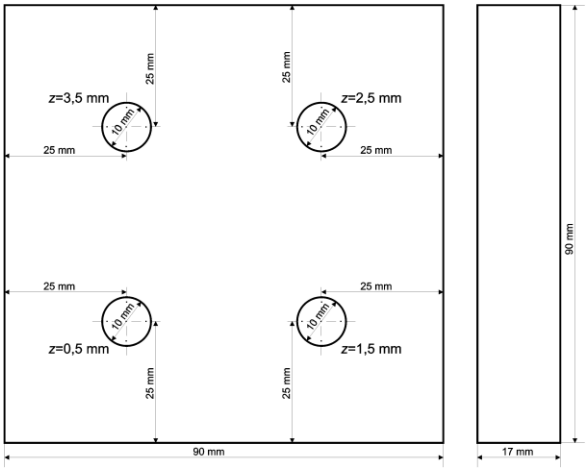

Fig. 3. Sample dimensions and location of holes simulating material defects [10].

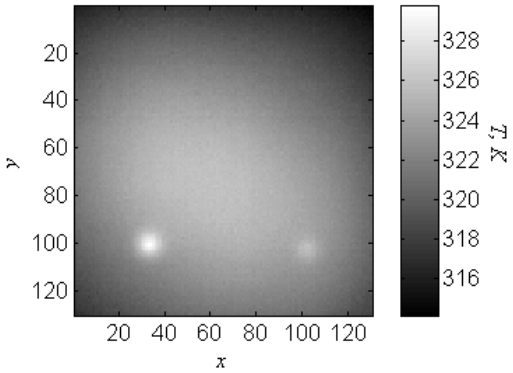

Fig. 4. Thermogram of sample surface for time instant $\tau = 32.8$ s (beginning of the heating stage).

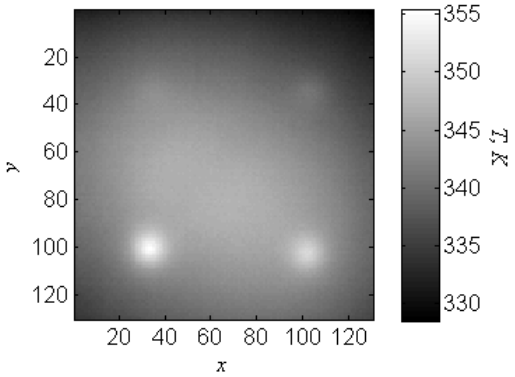

Fig. 5. Thermogram of sample surface for time instant $\tau = 120$ s (end of the heating stage).

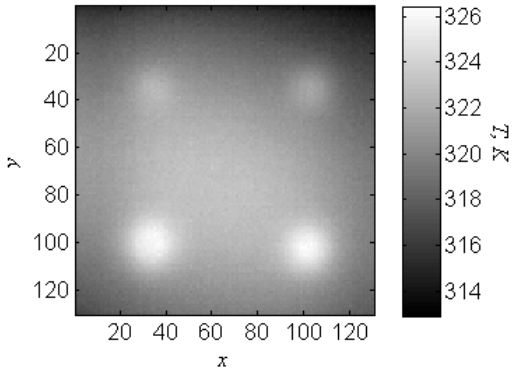

Fig. 6. Thermogram of sample surface for time instant $\tau = 240$ s (end of observation of the cooling stage).

3. Simulation tests

3.1. Methodology

In order to estimate the influence of correction on the effectiveness of defect detection, simulation tests of the described method for different options of approximation were carried

out. In the first sequence the influence of the choice of the time instant, *i.e.* the choice of the proper sequence thermogram, was examined. The simulation tests were carried out for thermograms recorded during experiments described in the previous part of the present work (Figs 4–6). Taking into account that the field of view for thermograms recorded during experiments was equal to 130 x 130 pixels, in the paper the grid size was assumed to be equal to 26 x 26 approximation nodes, what corresponds to sampling by 5 pixels in the x and y directions.

The background approximation was carried out using polynomials (7), (8). The approximation accuracy was assessed by calculation of least-square error. In order to assess quantitatively the correction effectiveness a simple statistical analysis was applied. For each option of the method the values of standard deviation along the horizontal and vertical temperature profile were calculated. Test profiles were situated at height (horizontal profile) and width (vertical profile) halves of the field of view.

During simulation tests, a conversion of the matrix of temperatures representing thermal images of the examined sample surface into intensity images was carried out, according to the following expression:

$$J(x,y)=\frac{255}{T_{\max}-T_{\min}}\left[T(x,y)-T_{\min}\right], \tag{14}$$

where: $J(x, y)$ – brightness level at the point with coordinates (x, y) for the intensity image, corresponding to the point of thermogram sequence with coordinates (x, y) and temperature $T(x, y)$, $T_{\max}$ – maximum value of temperature in the thermogram field of view, $T_{\min}$ – minimum value of temperature in the thermogram field of view. It should be noted that thermogram conversion into intensity images was carried out only for binarization purposes. The conversion is not a constituent of the described correction method. This method requires only "raw" thermograms of the examined surface. The last stage of simulation tests was Otsu binarization applied to thermograms before and after correction for individual cases. On the basis of binarization it was possible to compare different options of the proposed correction method and to assess their influence of the effectiveness of defect detection.

3.2. Simulation test results

3.2.1. Early heating stage (τ = 32.8 s)

In Figs 7–16 simulation test results carried out for the thermogram from Fig. 4, recorded in the early heating stage (τ = 32.8 s) are given. The results of correction of heating non-homogeneity with the use of background approximation (formula 7) are presented in Figs 7–12. In Fig. 7 the result of approximation of thermal background is depicted. The results of correction of heating non-homogeneity with marked test profiles are given in Fig. 8. Temperature distributions along test profiles are presented in Fig. 9 for the original thermogram and in Fig. 10 for the corrected thermogram, respectively. In Figs 11 and 12 the results of binarization are depicted, for the original and for the corrected thermogram, respectively. The results of background approximation with the relationship (8) are given in Figs 13–16. The approximated background is depicted in Fig. 13, whereas in Figs 14–16 the corrected thermogram, temperature distribution along test profiles after correction and the binarization result after correction are shown, respectively.

Metrol. Meas. Syst., Vol. XVII (2010), No. 4, pp. 00–00

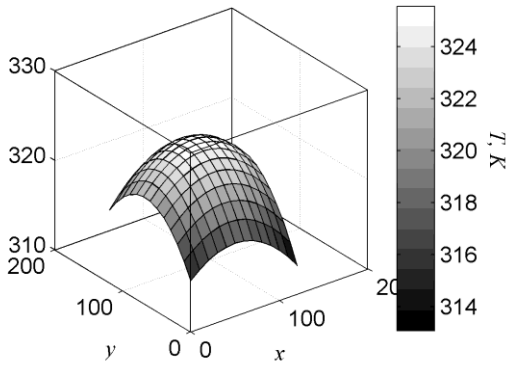

Fig. 7. Result of background approximation with formula (7).

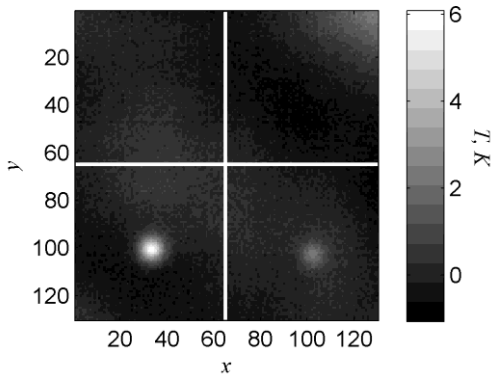

Fig. 8. Correction result with marked test profiles – approximation with formula (7).

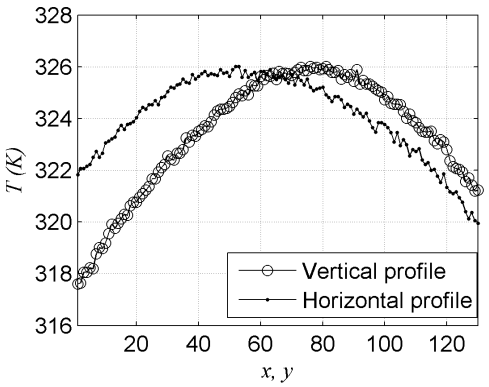

Fig. 9. Temperature distribution along test profiles of the original thermogram (τ = 32.8 s).

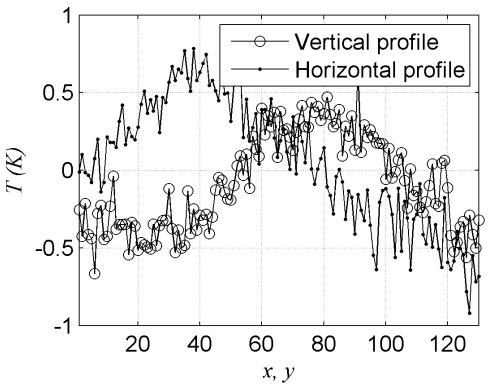

Fig. 10. Temperature distribution along test profiles after correction – approximation with formula (7).

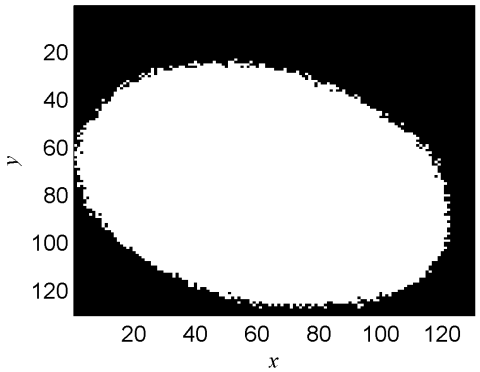

Fig. 11. Binarization result of the original thermogram (τ = 32.8 s).

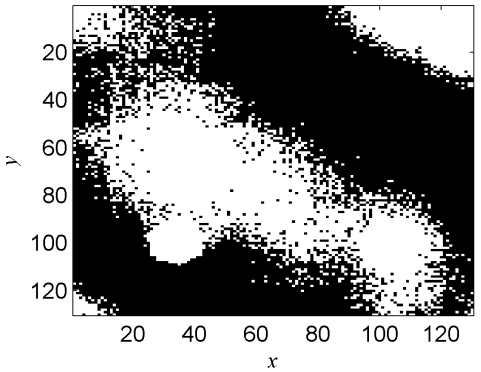

Fig. 12. Binarization result of the corrected thermogram – approximation with formula (7).

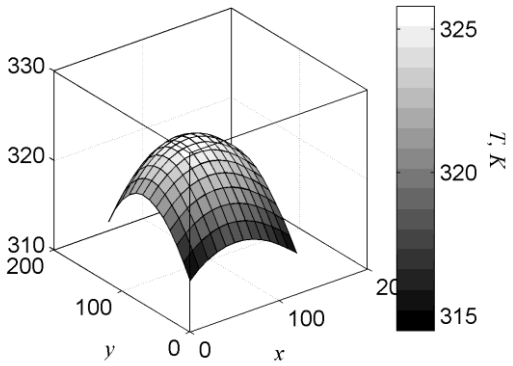

Fig. 13. Result of background approximation with formula (8).

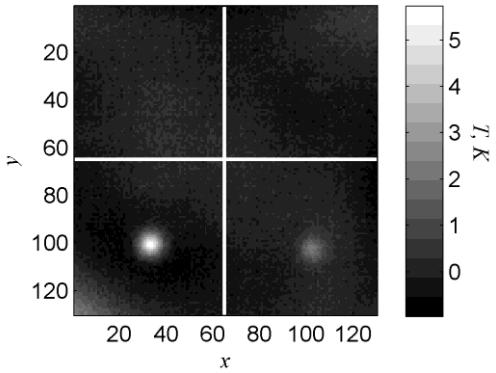

Fig. 14. Correction result with marked test profiles – approximation with formula (8).

3.2.2. End of heating stage (τ = 120 s)

In Figs 17–26 the results of simulations carried out for the thermogram from Fig. 5, recorded at the end of the heating stage (τ = 120 s) are presented in Figs 17–22. In Figs 17–22, the results of approximation of thermal background using formula (7) is depicted. The result of correction of heating non-homogeneity with marked test profiles is shown in Fig. 18. Temperature distributions along test profiles are presented in 19 for the original thermogram, and in Fig. 20 for the corrected thermogram, respectively. In Figs 21 and 22 the binarization results are presented, respectively for the original thermogram and for the thermogram after heating non-homogeneity correction.

Background approximation results with formula (8) are shown in Figs 23–26. The approximated background is presented in Fig. 23, whereas Figs 24–26 depict, respectively, the thermogram after correction, temperature distribution along test profiles for the thermogram after correction and the result of thermogram binarization after correction.

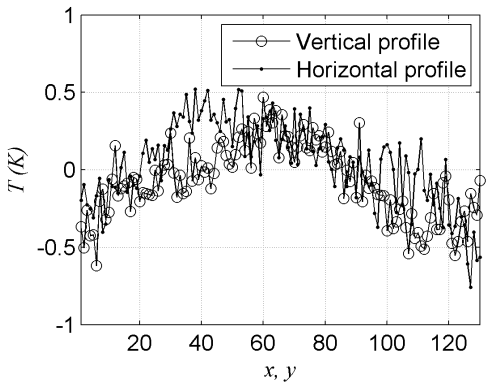

Fig. 15. Temperature distributions along test profiles for the thermogram after correction – approximation with formula (8).

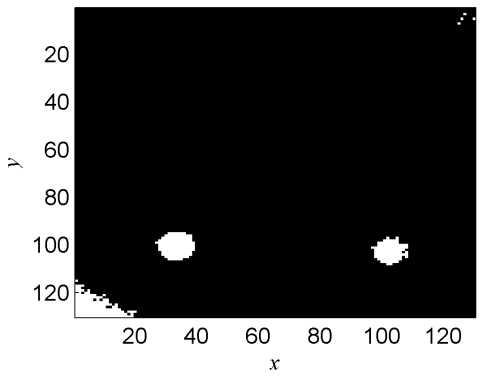

Fig. 16. The result of binarization of thermogram after correction – approximation with formula (8).

Metrol. Meas. Syst., Vol. XVII (2010), No. 4, pp. 00–00

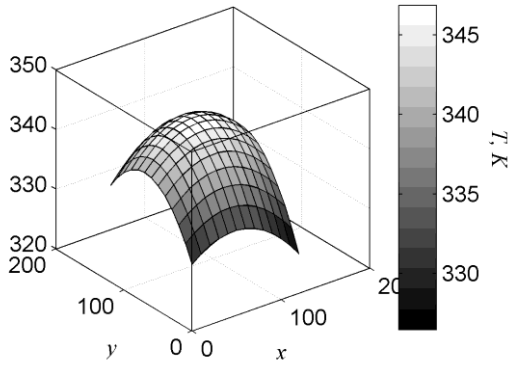

Fig. 17. Result of background approximation with formula (7).

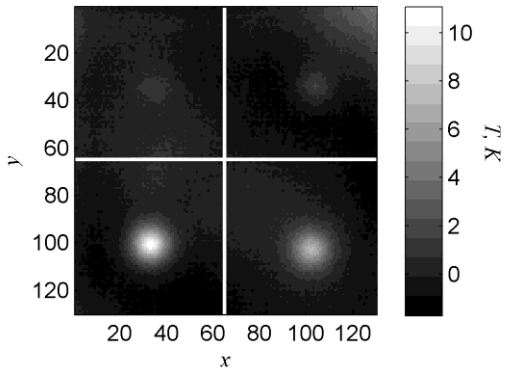

Fig. 18. Result of correction with marked test profiles – approximation with formula (7).

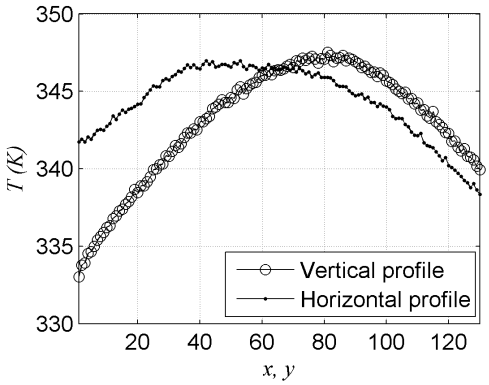

Fig. 19. Temperature distribution along test profiles for the original thermogram (τ = 120 s).

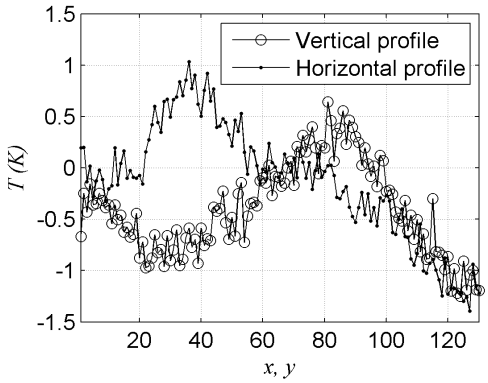

Fig. 20. Temperature distribution along test profiles after correction – approximation with formula (7).

3.2.3. Half of observation time during the cooling stage (τ = 180 s)

In Figs 27–36 the results of simulations carried out for the thermogram from Fig. 6, recorded for half of the observation time during the cooling stage (τ = 180 s) are given. The results of correction of heating non-homogeneity with the use of background approximation carried out with the use of formula (7) are depicted in Figs 27–32. In Fig. 27 the result of approximation of the thermal background is shown.

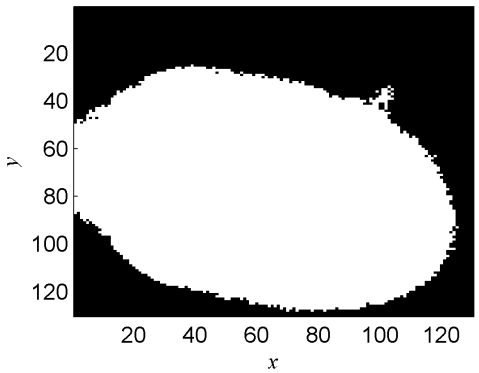

Fig. 21. Result of binarization applied to original thermogram (τ = 120 s).

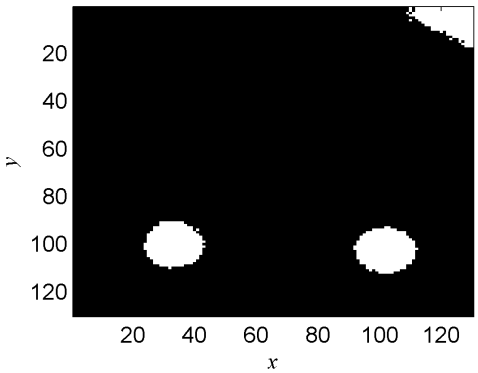

Fig. 22. Result of binarization applied to thermogram after correction – approximation with formula (7).

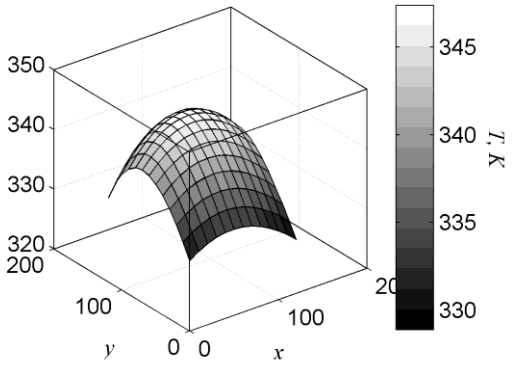

Fig. 23. Result of background approximation with formula (8).

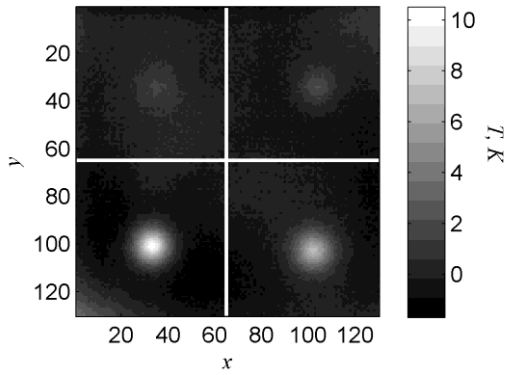

Fig. 24. Result of correction with marked test profiles – approximation with formula (8).

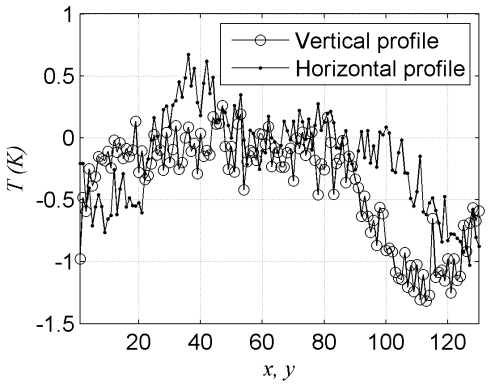

Fig. 25. Temperature distribution along test profiles for the thermogram after correction – approximation with formula (8).

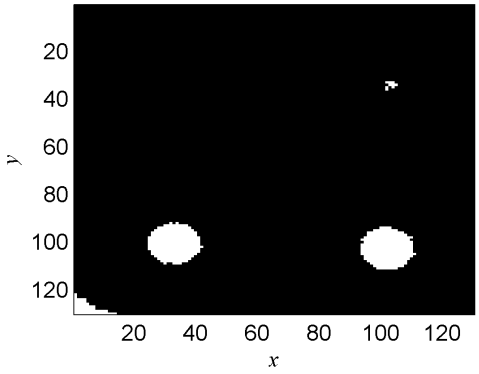

Fig. 26. Result of binarization applied to the thermogram after correction – approximation with formula (8).

The results of correction of heating non-homogeneity with marked test profiles are presented in Figure 28. Temperature distributions along test profiles are depicted in Figs 29 and 30 for the original thermogram and the thermogram after correction, respectively. In Figs 31 and 32 the binarization results are given for the original and the corrected thermogram, respectively. The results of background approximation using formula (8) are presented in Figs 33–36. The approximated background is shown in Fig. 33, whereas Figs 34–36 depict: thermogram after correction, temperature distribution along test profiles for the termogram after correction and the result of thermogram binarization after correction, respectively.

3.2.4 Assessment of approximation accuracy and correction effectiveness

The results of analysis of thermal background approximation and effectiveness of heating non-homogeneity correction are compiled in Tables 1, 2. In Table 1 the values of mean square errors obtained during approximation of the thermal background using formulas (7), (8) are given. The errors are calculated for three afore-discussed stages of thermal process, *i.e.* for time instants $\tau = 32.8$ s, $\tau = 120$ s, $\tau = 180$ s. As mentioned earlier, for quantitative assessment of the accuracy of heating non-homogeneity correction, test temperature profiles were applied in the present paper. In Table 2 the values of standard deviations of temperature distribution obtained along test profiles for all above-discussed stages of the thermal process and both formulas applied for approximation of thermal background are compiled. Additionally, for each stage standard deviations along profiles for original thermograms were presented in the Table.

Metrol. Meas. Syst., Vol. XVII (2010), No. 4, pp. 00–00

Table 1. Values of mean square errors, obtained during approximation of thermal background with formulas (7), (8).

FORMULA TYPE	τ = 32.8 s	τ = 120 s	τ = 240 s
FORMULA (7)	0.2610	1.2946	0.5742
FORMULA (8)	0.1654	0.9964	0.5292

Table 2. Values of standard deviations of temperature distributions along vertical and horizontal test profiles with the use of formulas (7), (8).

		τ = 32.8 s		τ = 120 s		τ = 240 s	
		ORIGINAL	CORRECTED	ORIGINAL	CORRECTED	ORIGINAL	CORRECTED
FORMULA (7)	VERT. PROFILE	2.285	0.306	3.748	0.444	1.989	0.184
	HORIZ. PROFILE	1.607	0.407	2.330	0.572	1.096	0.294
FORMULA (8)	VERT. PROFILE	2.285	0.241	3.748	0.418	1.989	0.275
	HORIZ. PROFILE	1.607	0.266	2.330	0.381	1.096	0.238

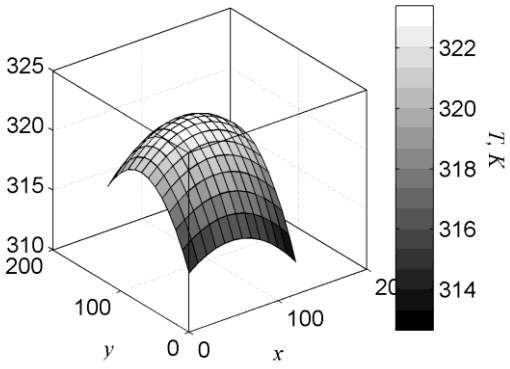

Fig. 27. Result of background approximation with formula (7).

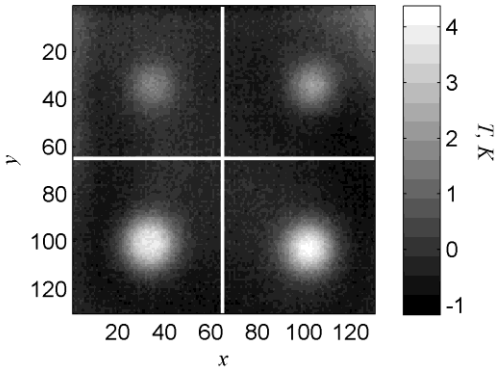

Fig. 28. Result of correction with marked test profiles – approximation with formula (7).

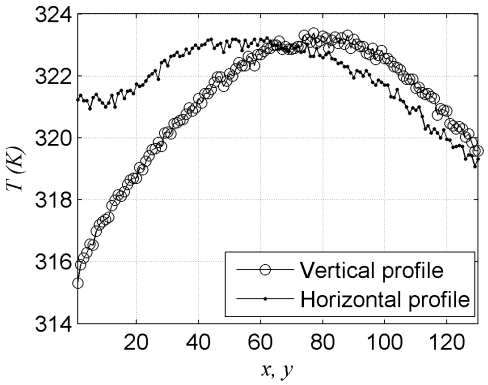

Fig. 29. Temperature distribution along test profiles for the original thermogram (τ = 180 s).

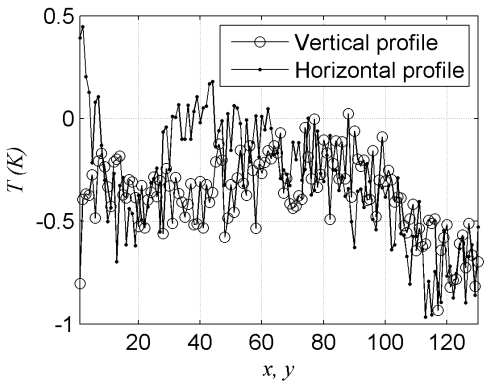

Fig. 30. Temperature distribution along test profiles for the corrected thermogram – approximation with formula (7).

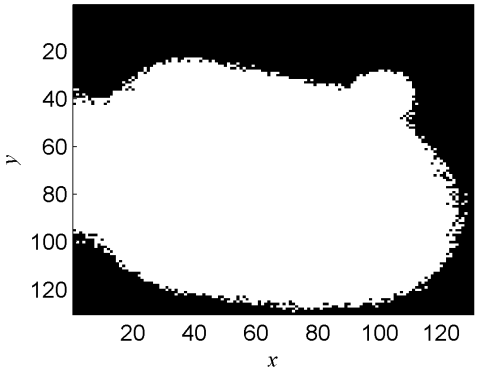

Fig. 31. Result of binarization of the original thermogram (τ = 180 s).

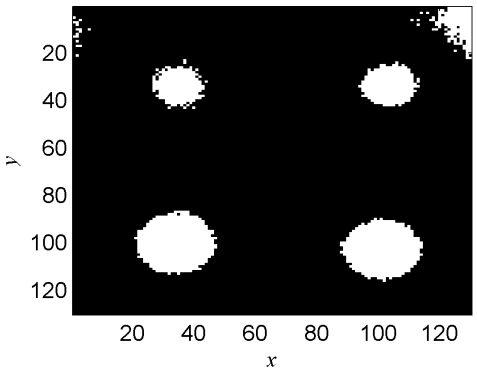

Fig. 32. Result of binarization of the thermogram after correction – approximation with formula (7).

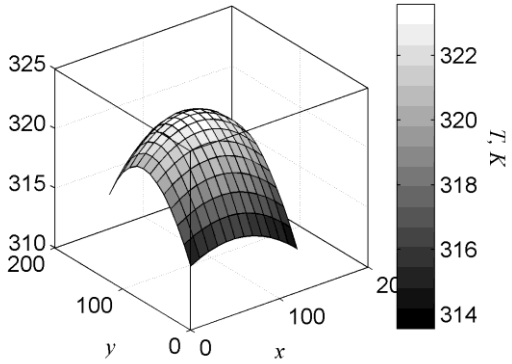

Fig. 33. Result of background approximation with formula (8).

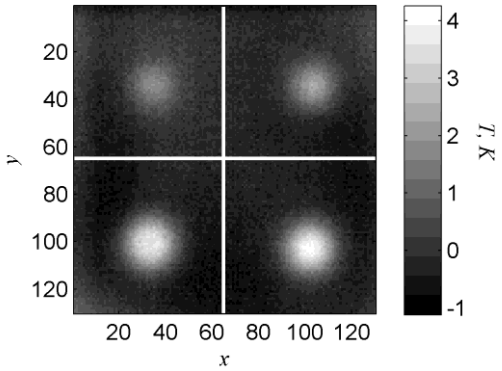

Fig. 34. Result of correction with marked test profiles – approximation with formula (8).

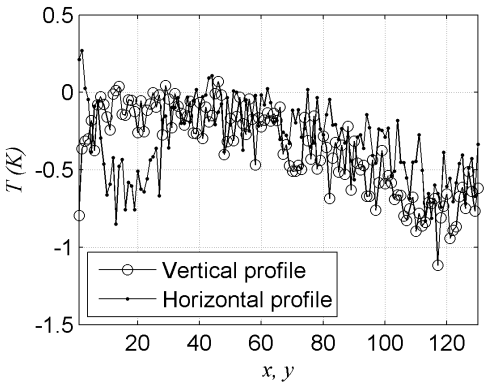

Fig. 35. Temperature distribution along test profiles for the termogram after correction – approximation with formula (8).

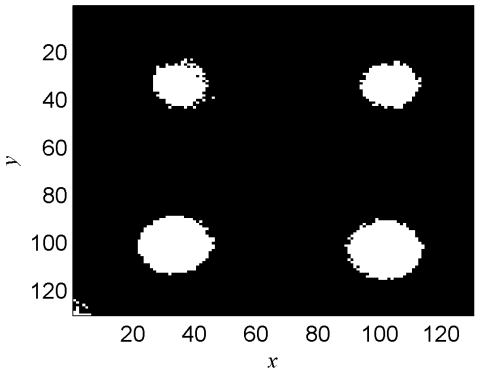

Fig. 36. Result of binarization for the termogram after correction – approximation with formula (8).

4. Conclusions

In the present paper a method useful for correction of heating non-homogeneity on the surface of a test sample which includes subsurface material defects, has been presented. Experimental and simulation-based tests of the proposed method have been carried out. During experimental tests, the stepped heating method has been applied. Simulation-based tests have been carried out for two formulas (polynomials), which approximated the thermal

background. Analyzing the results of experimental tests, the following conclusions may be drawn:

– In Figs 4–6 thermograms recorded for three time instants have been presented. Taking into account the location and depth of simulated defects it may be stated that in order to detect defects lying deeper it was necessary to increase the heating time of the examined sample.
– Non-uniform heating of the examined sample (non-homogenous thermal background) has been observed both in the heating and the cooling stages (Figs 4–6).
– In the experimental conditions considered in the present work, the defects visible in the thermogram of sequence recorded for time instant $\tau = 180$ s exhibited the highest contrast (Fig. 6).

Analyzing the results of simulation tests, the following conclusions have been formulated:

– During experimental tests, in order to increase heating homogeneity, two heating lamps of equal power have been used. Nonetheless the simple binarization method does not allow one for defect detection with the use of the original thermograms at any stage of the considered process. As can be seen from Figs 11, 21, 31, all defects visible in original thermograms are masked by heating non-uniformity of the test sample surface.
– In the present work it was found necessary to introduce a parameter which considered the heating non-homogeneity quantitatively. It was assumed that for comparison purposes, the standard deviation of temperature distributions along the vertical and the horizontal test profile could be such a parameter.
– Analyzing the data in Table 2, it can be stated that in the case of thermograms without correction the highest heating non-homogeneity occurs for time instant $\tau = 120$ s (end of heating stage), whereas at the beginning of the heating stage and at half of the cooling stage the non-homogeneity is much smaller. This results from the course of the thermal process.
– In any analyzed option (stage of thermal process, order of equation approximating the thermal background) the described method has significantly reduced the surface heating non-homogeneity, expressed as standard deviation of temperature distribution along test profiles. For example, at time instant $\tau = 120$ s and for approximation of thermal background with formula (8), the standard deviation along the vertical thermogram profile has been reduced approximately nine times, *cf*. Table 2. For this case the correction effect may be noticed from a comparison of Figs 19 and 25.
– From the point of effectiveness of the proposed method used for correction of heating non-homogeneity, a very important issue is the proper choice of thermogram sequence (choice of the proper time instant), as the contrast, which allows for defect detection, depends on time. From a comparison of binarization results pertaining to thermograms after correction it can be noticed that the highest effectiveness of defect detection has been obtained for the thermogram recorded at time instant $\tau = 180$ s, *cf*. Figs 32, 36.
– Analyzing the values of mean square errors compiled in Table 1, it should be stated that for time instants $\tau = 32.8$ s and $\tau = 120$ s, higher approximation accuracy is obtained when one uses formula (8). For time instant $\tau = 120$ s, for both formulas (7), (8) a comparable approximation accuracy is obtained, *cf*. Table 1.
– The effectiveness of heating non-homogeneity correction, thus the effectiveness of defect detection with the proposed method depends on the form of equation used for thermal background approximation. The highest differences in effectiveness are observed for relatively low contrast of defect imaging and high heating non-homogeneity at the same time. Such case occurs for time instant $\tau = 32.8$ s. As can be noticed from Fig. 4, the defects occurring in the original thermogram are depicted with a very low contrast. It follows that these are located too deeply. Actually, the only visible defect is the most

shallow one (z = 0.5 mm), *cf*. Fig. 3. Additionally, at this stage of the thermal process a high thermal non-homogeneity of test sample surface may be observed. Time instant τ = 32.8 s has been chosen intentionally. This is the first time instant for which the correction with formula (8) allows one to detect two most shallow defects, *cf*. Fig. 16. In this case, an increase of the order of approximation polynomial made it possible to obtain a better fit of this polynomial to the real thermal background. Approximation of thermal background with formula (7) at this stage of thermal process does not yield correct results, what may be concluded from a look at Fig. 12.

References

[1] Minkina, W., Dudzik, S. (2009). *Infrared Thermography – Errors and Uncertainties.* Chichester, John Wiley & Sons.

[2] Minkina, W. (2004). *Thermovision Measurements – methods and instruments.* Czestochowa: Publishing Office of Czestochowa University of Technology. (in Polish)

[3] Madura ,H., *et al*. 2004 Thermovision measurements in practice. PAK Publishers Agenda. (in Polish)

[4] Minkina, W., Dudzik, S. (2006). Simulation analysis of uncertainty of infrared camera measurement and processing path. *Measurement*, 39(8), 758-763.

[5] Dudzik, S. (2005). Analysis of influence of correlation coefficient between measurement model input variables on uncertainty of temperature determination with an infrared camera. In *Proceedings of XXXVII MKM conference*. Zielona Góra, 195-203. (in Polish)

[6] Dudzik, S., Minkina, W. (2008). Application of the numerical method for the propagation of distributions to the calculation of coverage intervals in the thermovision measurements. In *Proceedings of 9th Conference on Quantitative Infrared Thermography*. Kraków, 179-184.

[7] Maldague, X.P. (2001). *Theory and practice of infrared technology for nondestructive testing*. New York: John Wiley & Sons Interscience.

[8] Gleiter, A., Spiessberger, C., Busse, G. (2008). Phase angle thermography for depth resolved characterization. In *Proceedings of 9th International Conference on Quantitative Infrared Thermography QiRT*, Kraków, 435-441.

[9] Zöcke, C., Langmeier, A., Stössbel, R., Arnold, W. (2009). Reconstruction of the defect shape from lock-in thermography phase images. *QIRT Journal*, 6(1), 63-78.

[10] Dudzik, S. (2009). A simple method for defect area detection using active thermography. *Opto-Electronics Review*, 17(4), 338-344.

[11] Dudzik, S. (2010). Application of the morphological operations for defect area recognition using active thermography. In *Proceedings of 10th Conference on Quantitative Infrared Thermography*. Université Laval, Québec. (in press)

[12] Fourier, J. Théorie du mouvement de la chaleur dans les corps solides-2 Partie. *Mémoires de l'Academie des Sciences*, 5(153), 1826.

[13] Carlslaw, H.S., Jaeger, J.C. (1959). *Conduction of heat in solids*. 2nd ed. New York: Oxford University Press.

[14] Russ, J.C. (2002). *Image Processing Handbook*. CRC Press LLC.

[15] Burden, R.L., Faires, J.D. (2004). *Numerical analysis*. 8th ed. Brooks Cole.

[16] Malina, W., Smiatacz, M. (2008). *Digital image processing*. Warsaw: Academic Publishing Office EXIT. (in Polish)

[17] Nieniewski M. (2005). *Segmentation of Digital images. Watershed segmentation methods*. Warsaw: Academic Publishing Office EXIT. (in Polish)